Paper ID: CE-0318

Effect of Minor Groin on the Downstream Groin Area

T. Ali[1], M. Alauddin[1], J. Alam[1], S. Hossain[1], M. Hossain[1]

[1] Department of Civil Engineering, DUET, Bangladesh (*tulahmmed@gmail.com)

Abstract

Riverbank erosion has been a disastrous phenomenon in Bangladesh causing damage to infrastructure, livelihood, and posing a threat to biodiversity and ecosystem services. To address the issue, various measures have been taken including the construction of groins, embankments, revetments, and so on. Groins slow down the flow along the shoreline to reduce erosion and protect the riverbank. However, they can be unstable due to toe scour. Many researchers have studied to stabilize the groin from toe scour, but no researcher ever worked with a minor combined groin. This study uses a two-dimensional numerical model, iRIC (Nays 2DH), to examine the changes in hydraulic and morphological characteristics in a sand-bed channel due to a minor groin. First, the effect of flow on the groins of conventional arrangement is examined, and then a minor groin is employed upstream with three different configurations such as (i) a minor impermeable groin, (ii) a minor permeable groin, and (iii) a minor combined groin to minimize the effect. From the simulated results, this can be concluded that a minor combined groin gives the best result in minimizing the flow vortices near the first groin and reducing scour near the groin head. This finding can help engineers, designers, and policymakers to find a long-term solution to the groin destabilization problem.

Keywords: *Erosion; local sour; minor groin; combined groin; iRIC.*

1 Introduction

The majority of the materials that make up Bangladesh's riverbanks and beds are alluvial materials that the rivers themselves have carried and deposited. Bank soils are eroded during the monsoon season due to excessive water discharge. The river's flow diminishes during the dry season as a result of a lack of rainfall and excessive water withdrawals from the adjacent upstream countries, which results in sedimentation and a reduction in the river's depth. Every year, rivers in Bangladesh erode about 10,000 hectares of land (Islam and Rashid, 1970). The left bank of the Jamuna River was found to be eroding at a pace of 227 m/year in prior research (Baki and Gan, 2012). Several structures have been constructed to stop banks from eroding, including permeable groins at Kamarjani, guide banks for the Bangabandhu Bridge, town protection revetments in Sirajganj and Bhuapur, hard points at Sariakandi and Mathurapara, and groins at Kalitola and Bahadurabad. Among these structures, groins are more effective to protect river bank erosion.

Although the groins are effective river training structures over others, they fail when there is persistent erosion at their landward end, which leads to the groin becoming detached and enabling sand and water to enter through the groin (Bush et al, no date). Another reason for the failure of the groin is oblique flow. Oblique flow removes bed material from the launching apron, then the launching apron is displaced and the groin is failed through slip circle failure (Nazim Uddin, 2010). Many methodologies have been taken to stabilize the groins using different materials, changing the projection angle, length, and spacing of the groins. According to (Krishna Prasad, Indulekha and Balan, 2016), the cocolog groin might be utilized to increase center line velocity and water levels on the upstream side for navigational reasons. An angle of 135^0 was determined to provide the best protection. I. Khassaf and A. Abbas, 2018 found through their research that the scour depth decreased with increasing the number of groins by about 3.33 – 30.2% for each increase in the number of groins equal to one, and the distances between them by about 3.13-17% for each half of the groin length increase in these distances. The strength of the secondary flow around the T-shaped spur dike was reduced by 50% by the support structure (Impermeable minor groin). The support structure enhanced the separation zone and reduced the maximum velocity by up to 12% in the area surrounding the T-shaped spur dike. The separation zone's length grows linearly when the support structure's distance is increased. In the model with a distance of 5*L* (*L* is the length of the T-shape spur), the separation zone's

maximum width was documented. When the support structure's distance advances, the separation zone's width escalates nonlinearly (Vaghefi et al, 2015). After reviewing the earlier studies, it was clear that no one had previously researched the effect of the minor combined groin. The present study has assessed the impact of minor impermeable, permeable, and combined groins to improve the hydro-morphological characteristics in the area of downstream major groins. This study used a 2D numerical model called iRIC (Nays2DH), which is based on Navier-Stokes equations, to simulate the flows and sediment transport in an open channel with groin models. The goal of the research is to track the hydrodynamic and morphological modifications made to the river channel as a result of the groin installation. The first groin has higher local scours, which is ultimately led to the structural breakdown. A minor groin upstream could be able to solve the issue by reducing the hydraulic action on the conventional groin. The following specific objectives are considered to minimize the effects of upstream flow on the groins.

a) To determine the hydraulic and morphological characteristics in the open channel due to the interaction of groins.
b) To investigate the effect of minor impermeable, permeable, and combined groins on the downstream groin area.

.

2 Methodology

2.1 Equations Used in the Numerical Model

Basic Equations

Continuity equation:

The horizontal momentum equations of flow and the continuity equations make up the set of equations controlling the flow. In an orthogonal coordinate system (x,y), the fundamental equations are as follows:

$$\frac{\partial h}{\partial t}+\frac{\partial (hu)}{\partial x}+\frac{\partial (hv)}{\partial y}=0 \quad (1)$$

Momentum equations in x and y-directions:

$$\frac{\partial (uh)}{\partial t}+\frac{\partial (hu^2)}{\partial x}+\frac{\partial (huv)}{\partial y}=-gh\frac{\partial H}{\partial x}-\frac{\tau_x}{\rho}+D^x+\frac{F_x}{\rho} \quad (2)$$

$$\frac{\partial (vh)}{\partial t}+\frac{\partial (huv)}{\partial x}+\frac{\partial (hv^2)}{\partial y}=-gh\frac{\partial H}{\partial y}-\frac{\tau_y}{\rho}+D^y+\frac{F_y}{\rho} \quad (3)$$

In which

$$\frac{\tau_x}{\rho}=C_f u\sqrt{h^2+v^2} \qquad \frac{\tau_y}{\rho}=C_f v\sqrt{h^2+v^2}$$

$$D^x=\frac{\partial}{\partial x}\left[v_t h\frac{\partial u}{\partial x}\right]+\frac{\partial}{\partial y}\left[v_t h\frac{\partial u}{\partial y}\right] \qquad D^y=\frac{\partial}{\partial x}\left[v_t h\frac{\partial v}{\partial x}\right]+\frac{\partial}{\partial y}\left[v_t h\frac{\partial v}{\partial y}\right]$$

$$\frac{F_x}{\rho}=\frac{1}{2}C_D a_s h_v u\sqrt{u^2+v^2} \qquad \frac{F_y}{\rho}=\frac{1}{2}C_D a_s h_v v\sqrt{u^2+v^2}$$

where g is gravitational acceleration, h is water depth, τ_x and τ_y are the components of the shear stress of the river bed in the *x*- and *y*-direction, *t* is time, *u* and *v* are depth-averaged velocities in the *x*- and *y*-directions, and F_x and F_y are parts of the vegetation's drag force in the *x*- and *y*-direction, respectively. C_f is the drag coefficient of the bed shear stress, v_t is the eddy viscosity coefficient, C_D is the drag coefficient of the vegetation, together with the area of interception by the vegetation per unit volume, and h_v is the minimum value of the water depth and height of the vegetation.

Equations for Bed Load Transport

The total bedload transport qb in the depth-averaged velocity direction (in the direction of *V*) is estimated using Ashida and Michiue formula as follows:

$$q_b=17\tau_e^{1.5}\left(1-k_c\frac{\tau_{*c}}{\tau_c}\right)\left(1-\sqrt{k_c\frac{\tau_{*c}}{\tau_c}}\right)\sqrt{s_d g d^3 r_b} \quad (4)$$

where effective Shields number is calculated as follows,

$$u_{*c}^2 = \frac{V^2}{\left(6+2.5ln\frac{h}{d(1+2\tau_*)}\right)^2}$$
$$\tau_{*c} = \frac{u_{*c}^2}{sgd}$$

where τ_{*c} is critical Shields number which is calculated by Iwagaki formula. K_c is the modification function of the effect of the local bed slope on the sediment transport as follows:

$$K_c = 1 + \frac{1}{\mu_s}\left[\left(\frac{\rho}{\rho_s-\rho}\right)\cos\alpha\tan\theta_x + \sin\alpha\tan\theta_y\right]$$

where α is the angle of deviation of near-bed flow from *x*-direction and defined as follows,

$\alpha = arctan\left(\frac{v_b}{u_b}\right)$

μ_s is the static friction coefficient of bed material. θ_x and θ_y are bed inclinations in the x and y-directions, respectively. These inclinations are evaluated as follows:

$$\theta_x = arc\tan\left(\frac{\partial\xi}{\partial x}\frac{\partial z_b}{\partial\xi} + \frac{\partial\eta}{\partial x}\frac{\partial z_b}{\partial\eta}\right) \qquad \theta_y = arc\tan\left(\frac{\partial\xi}{\partial y}\frac{\partial z_b}{\partial\xi} + \frac{\partial\eta}{\partial y}\frac{\partial z_b}{\partial\eta}\right)$$

Equations for Upward Flux of Suspended Load from River Bed

For measuring the upward flux of suspended load from river bed, Itakura and Kishi formula is used which are represented as follows:

$$q_{su} = K\left[a_*\frac{\rho_s-\rho}{\rho_s}\cdot\frac{gd}{u_*}\Omega - w_f\right]r_b \qquad (5)$$
$$\Omega = \frac{\tau_*}{B_*}\cdot\frac{\int_{a'}^{\infty}\xi\frac{1}{\sqrt{\pi}}exp[-\xi^2]d\xi}{\int_{a'}^{\infty}\frac{1}{\sqrt{\pi}}exp[-\xi^2]d\xi} + \frac{\tau_*}{B_*\eta_o} - 1$$
$$a' = \frac{B_*}{\tau_*} - \frac{1}{\eta_o},\ \eta_o = 0.5,\ a_* = 0.14,\quad k = 0.008$$

where q_{su} is the upward flux of suspended load from river bed and w_f is the settling velocity of suspended sediment, which is obtained with Rubey's equation. B^* is a conversion factor for applying friction velocity to the velocity in lift force calculation. The constant value of B^*= 0.143 is used in the case of uniform grain size.

2.2 Model Setup

The region being modeled is a schematized straight channel reach that is 8 meters long (*L*), 1.5 meters wide (*B*), and has a slope of S_0 = 0.001. While maintaining a consistent channel width, the bed was treated as moveable. For calculation, the channel was split into 30 grids in the transverse direction and 160 grids in the longitudinal direction. The flow is in the x-direction, with *x* = 0 marking the position of the first conventional groin, while the *y*-axis is transversely oriented, pointing to the left bank. The study first takes into account four conventional groins. Each groin is 0.45 m (L_g) long, 1.125 m (S_g) apart, and has an aspect ratio of 2.5 (S_g/L_g). Three alternative minor groin models are adopted to place at the upstream side to minimize the effect of flow. The conventional groin model without a minor groin is configured as shown in Figure 2.2 (a) (Case 1). The configuration of the groins with an impermeable minor groin (Case 2) at 0.6 m upstream of the first conventional groin with a length of 0.3 m (L_{gm}) is depicted in Figure 2.2. (b). The conventional groin still has the same size and shape as before. In addition to four conventional groins, a minor permeable groin of length 0.25 m (L_{gm}) with 40% opening is used (Case 3), and a minor combined groin of length 0.3 m (L_{gm}) whose first 33.33% of length is impermeable and the rest 66.67% of length is permeable with 50% openness is adopted (Case 4). The conventional groin configuration and specification remain the same as in Case-2. Figure 2.2. (c) and Figure 2.2. (d) are shown the configuration and orientation of Case-3 and Case-4. All the groins are oriented 90^0 with bank reach for all Cases.

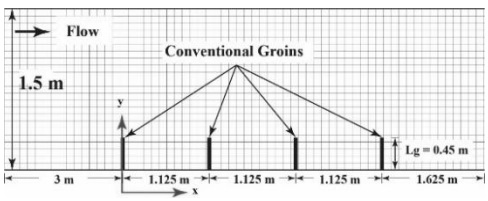

(a) Case-1

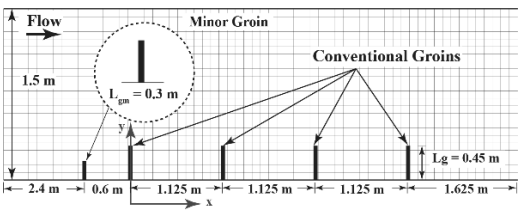

(b) Case-2

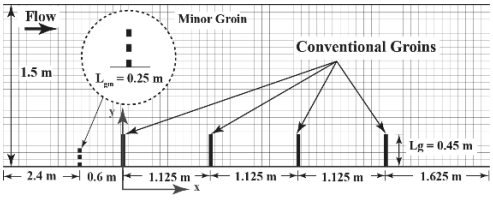

(c) Case-3

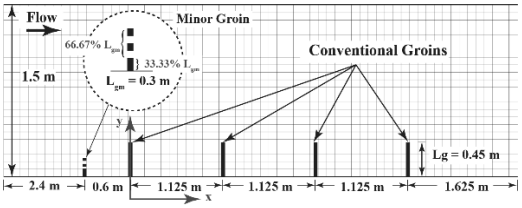

(d) Case-4

Figure 2.2.: Configuration of (a) Case-1 (b) Case-2 (c) Case-3 (d) Case-4

2.3 Simulation Condition

The Nays2DH computational model, which combines the Nays2D and Morpho2D solvers, has been utilized to analyze sediment movement, morphological changes of bed and banks, and horizontal two-dimensional flow. In the computation, idealized flow and sediment characteristics are taken into account. Velocity at upstream, initial water surface at upstream, and downstream is considered as uniform flow. Geographic information is used to compute the slope for uniform flow. Upstream water flow is assumed to be constant at 0.03 m^3/s (Q), and the upstream and downstream constraints each have a set water level of 0.1 m (H). With a time step of 0.005, each run is done for the period of t = 6 hours. For calculating bedload transfer, Ashida and Michiue's formula is used, and uniform bed material is assumed as 0.00015 m. In this study, the roughness coefficient is assumed to be n = 0.02 and the effect of roughness is computed using Manning's equation. For assessing turbulent flow that incorporates eddies of varying sizes and structures, the zero equation model is taken into account. Using Itakuara and Kishi's formula, the upward flow of the suspended load is measured. To estimate vegetative resistance, the drag coefficient is assumed to be 0.7.

3 Results and Discussions

To understand the hydraulic and morphologic characteristics and adopt the most effective groin model, velocity and bed deformation are outlined in this part. The model was first validated using experimental data (Rajaratnam and Nwachukwu, 1983), but is not included here. The groin model is assessed by taking into account scour depth and velocity. Following is a description of velocity and scour depth at various sections for several models:

3.1 Hydraulic Characteristics

According to the computation's findings, the flow is constrained when groins incorporate the channel, which causes the flow in the main channel to accelerate. Case-3 has a greater accelerated main channel velocity. Figure 3.1.1(f) displays this velocity in the contour. For various groin models, there are variations in the degree of skewness. The flow velocity is larger for the conventional groin at point *x*/*L*g = -1.22 since there isn't a minor groin blockage. However, a minor groin obstruction prevents Cases-2,3 and 4 from flowing, resulting in a steady flow close to the bank. Cases-3 and 4 have the highest and lowest measured velocities, respectively, as illustrated in Figure 3.1.2 (a) where V is the actual velocity and v is the average velocity. The greatest velocity for Case-4 appears at *y*/*L*g = 1.44, positioned *x*/*L*g = 0.22. The velocity is 15.5% greater at this point than it is with Case-1. The minor combined groin's impermeable portion resists the flow but permeable portions allow some portion of the flow to pass through. This passing flow is then opposed by the first traditional groin, which diverts the flow, but the separation isn't great, therefore the velocity is higher.

Peak velocities for Case-3 and Case-4 are nearly identical. Because of varied flow concentration patterns, the peak positions are fluctuating. Case-3, which can be viewed in Figure 3.1.2 (a), has the lowest peak out of all the models. For the entire model, velocity is nearly nil up until the length of the groin. varied models have varied recirculation patterns as well. Figures 3.1.1 (a, b, c, and d) also depict the velocity vector for several models.

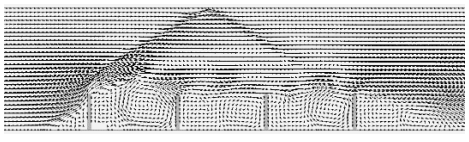

(a)

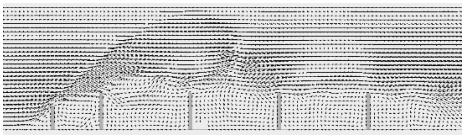

(b)

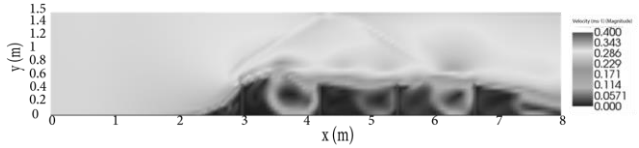

(e)

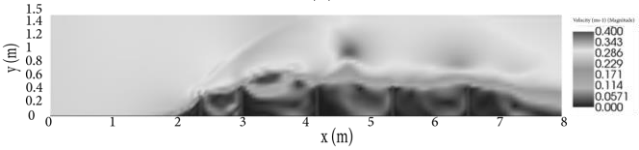

(f)

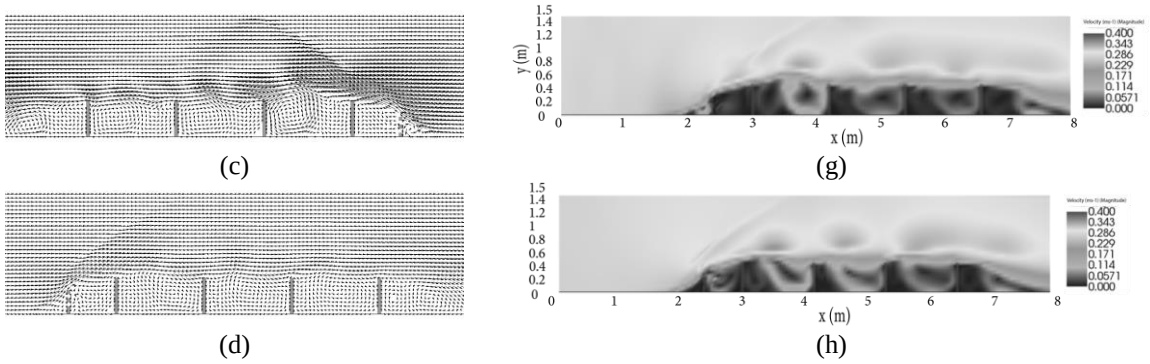

Figure 3.1.1: velocity vector and recirculation zone for (a) Case-1 (b) Case-2 (c) Case-3 (d) Case-4. (e) velocity contour for conventional groin model (f) velocity contour of Case-2 (g) velocity contour of Case-3 (h) velocity contour of Case-4

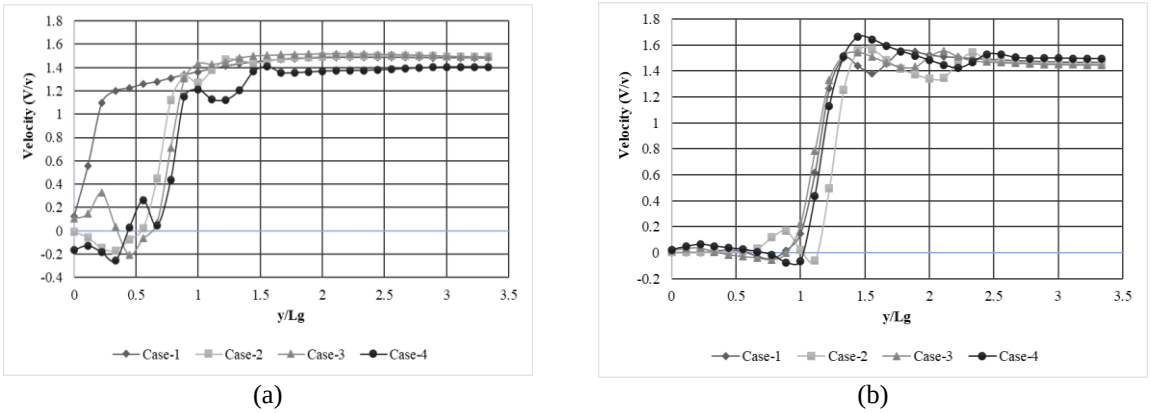

Figure 3.1.2: Comparison of resultant velocity profile (a) at x/L_g = -1.22 (b) at x/L_g = 0.22

3.2 Bed Changes

The primary problem with this study was that the local scour was greater for the conventional groin. Converging currents near groins provide localized pockets of faster water flow, which leads to scouring. Figure 3.2 (f) depicts the greatest scour, $\frac{\Delta Z}{H}$=1.1, which was discovered at a distance of y/Lg =1.44. The topographical view of bed changes were also shown in Figure 3.2 (a), (b), (c), (d) for Conventional groin, Case-2, Case-3, and Case-4. After deploying a minor groin, the scour depth downstream of the first conventional groin was significantly reduced. For Case-2, Case-3, and Case-4, respectively, scour was reduced by 10.1%, 22.18%, and 42.36%. The highest scour ($\frac{\Delta Z}{H}$=0.99) for the three models was measured for Case-2 at y/Lg = 1.89, as shown in Figure 3.2 (f). Results from Models 2 and 3 are pleasing. Figures 3.2(c) and (d) illustrate how the maximum scour formed distant from the groin tip. The local scour at the minor groin (x/Lg = -1.22) is minimal for Case-2 and largest for Case-3, whereas Case-4 yields the least scour of all the models. For Case-2, Case-3, and Case-4, correspondingly, the maximum scour is given as $\frac{\Delta Z}{H}$ = 1.32, 5.88, and 2.30. The currents that formed close to the permeable groin lead to the greatest local scour directly downstream of the minor groin, as shown in detail in Figures 3.2 (c) and 3.1.1 (c). The impermeable minor groin completely diverted water flow away from its tip, preventing currents from forming there and causing minimal erosion of the minor groin region. Finally, it is discovered after examining each model separately that Case-4 both reduces the scour depth and raises the mainstream velocity. In comparison to other models, scour is also significant towards the combined minor groin tip. Thus, it is evident that the conventional groin may be practiced in the field whenever a combined minor groin is used upstream.

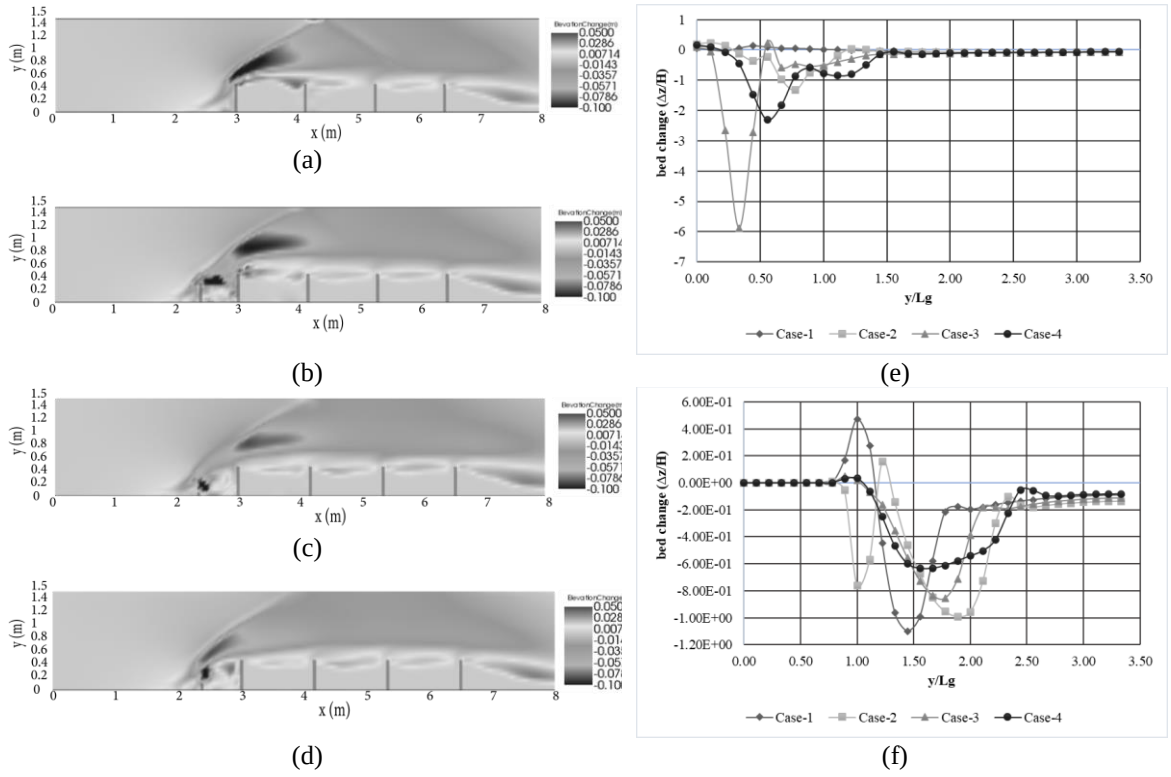

Figure 3.2: Contour of bed elevation change (a) Case-1 (b) for Case-2 (c) for Case-3 (d) for Case-4 (e) comparison of bed elevation change at x/L_g = -1.22 (f) comparison of bed elevation change at x/L_g = 0.22

4 Conclusion

The goal of this study was to identify an effective protection structure for the main impermeable groin. The velocity profile and variations in bed level were taken into account while evaluating the cases. Following is a summary of the conclusion drawn from the computed results:

i. The highest flow velocity at the middle stream was found for Case-4 and the lowest for Case-2.
ii. Local scour downstream of the minor groin is minimum for Case-2 but maximum for the downstream conventional groin.
iii. Scour is minimum for Case-4 in comparison to other models for both minor and conventional groin.

References

Baki, A.B.M. and Gan, T.Y. (2012) 'Riverbank migration and island dynamics of the braided Jamuna River of the Ganges-Brahmaputra basin using multi-temporal Landsat images', Quaternary International, 263, pp. 148–161.

Bush, D.M., Pilkey, O.H. and Neal, W.J. (no date) Coastal Topography, Human Impact on.

I. Khassaf, S. and A. Abbas, H. (2018) 'Study of the Local Scour Around L-Shape Groynes in Clear Water Conditions', International Journal of Engineering & Technology, 7(4.20), p. 271.

Islam, M.F. and Rashid, A.B. (1970) 'Riverbank erosion displacees in Bangladesh: need for institutional response and policy intervention', Bangladesh Journal of Bioethics, 2(2), pp. 4–19.

Krishna Prasad, S., Indulekha, K.P. and Balan, K. (2016) 'Analysis of Groyne Placement on Minimising River Bank Erosion', Procedia Technology, 24, pp. 47–53.

Nazim Uddin, M. (2010) Flow and erosion process at bends and around river training works in a sand bed braided river. A Ph.D. Thesis. Institute of Water and Flood Management, BUET.

Vaghefi, M., Ahmadi, A. and Faraji, B. (2015) 'The Effect of Support Structure on Flow Patterns Around T-Shape Spur Dike in 90° Bend Channel', Arabian Journal for Science and Engineering, 40(5), pp. 1299–1307.